



More frequent, persistent, and deadly heat waves in the 21st century over the Eastern Mediterranean

Marcel Wedler^a, Joaquim G. Pinto^a, Assaf Hochman^{a,b,*}

^a Institute of Meteorology and Climate Research, Department of Tropospheric Research (IMK-TRO), Karlsruhe Institute of Technology (KIT), Karlsruhe, Germany

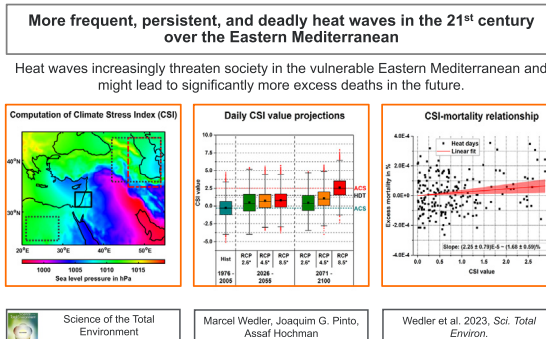
^b Fredy and Nadine Hermann Institute of Earth Sciences, The Hebrew University of Jerusalem (HUJI), Jerusalem, Israel



HIGHLIGHTS

- Significant intensification of heat stress projected for the Eastern Mediterranean.
- Heat wave duration, frequency, and severity are projected to increase.
- The persistence of heat days is projected to increase.
- Projected changes in heat stress are primarily attributed to temperature increases.
- Heat-related mortality may increase to ~330 deaths during Summer in Israel.

GRAPHICAL ABSTRACT



ARTICLE INFO

Editor: Jay Gan

Keywords:

Middle East
Dynamical systems
Extreme weather
Climate change
Public health
Mortality projection

ABSTRACT

Heat waves are extreme events characterized by sweltering weather over an extended period. Skillful projections of heat waves and their impacts on human mortality can help develop appropriate adaptation strategies. Here, we provide nuanced projections of heat wave characteristics and their effect on human mortality over the Eastern Mediterranean based on ERA5 reanalysis and CORDEX ensemble simulations. Heat waves were identified according to the 90th percentile threshold of the Climatic Stress Index (CSI), specifically tailored for the summer conditions in this region. We provide evidence that heat waves in the region are projected to occur seven times more often and last three times longer by the end of the 21st century (RCP8.5). We find that heat waves will become more persistent in a warmer world. Finally, we offer a conservative estimate of excess mortality in Israel based on a simple linear model. The projected changes in heat stress intensity and frequency may result in ~330 excess deaths per summer at the end of the 21st century (RCP8.5) compared to the historical baseline of ~30 heat-related deaths, particularly pronounced in the elderly (65+ years).

We conclude that heat waves increasingly threaten society in the vulnerable Eastern Mediterranean. We also emphasize that true interdisciplinary regional collaborations are required to achieve adequate public health adaptation to extreme weather events in a changing climate.

1. Introduction

Heat waves are hazardous weather events that affect many regions worldwide. While there is no universal definition of heat waves, they are generally defined as episodes of abnormally hot weather over a prolonged period characterized by wide-ranged impacts (Perkins and Alexander, 2013; Chen et al., 2015; Becker et al., 2022). Health effects include

* Corresponding author at: Fredy and Nadine Hermann Institute of Earth Science, The Hebrew University of Jerusalem, Jerusalem, Israel.

E-mail address: Assaf.Hochman@mail.huji.ac.il (A. Hochman).

<http://dx.doi.org/10.1016/j.scitotenv.2023.161883>

Received 4 November 2022; Received in revised form 23 January 2023; Accepted 24 January 2023

Available online 31 January 2023

0048-9697/© 2023 The Authors. Published by Elsevier B.V. This is an open access article under the CC BY-NC license (<http://creativecommons.org/licenses/by-nc/4.0/>).

increased mental and physical stress (Epstein and Moran, 2006; Lee et al., 2018) and morbidity (Åström et al., 2011). Finally, heat waves can increase excess mortality rates, particularly in risk groups such as the elderly (Åström et al., 2011; Chen et al., 2015). Notable examples of heat waves in recent years are the 2003 European heat wave, with 30,000–75,000 excess deaths in Europe (Robine et al., 2008), and the so-called ‘2010 Russian heat wave’, which caused about 55,000 deaths (Swiss Re Economic Research & Consulting, 2011). Other impacts include infrastructural damage, elevated electricity demands and power outages (Zimmerman and Faris, 2010; Zachariadis and Hadjinicolaou, 2014), impaired agricultural productivity (Deryng et al., 2014; Belhadj Slimen et al., 2016) as well as stress on ecosystems (Ruthrof et al., 2018; Wang et al., 2019).

Heat wave duration, frequency, and intensity have already increased in many regions worldwide (Coumou and Rahmstorf, 2012; Perkins and Alexander, 2013), and this trend is projected to intensify in the future (Russo et al., 2017; Mora et al., 2017). Addressing climate change at the regional scale, especially in regions of complex topography, such as the Eastern Mediterranean, requires data of high spatial resolution (Giorgi and Gutowski, 2015; Latt et al., 2022). Such resolutions can be obtained by dynamically downscaling global simulations with a regional climate model.

The Mediterranean region is a climate change ‘hotspot’ (Giorgi and Lionello, 2008) due to its location at the border between temperate and arid climates. This makes the region particularly susceptible to small changes in the general circulation (Giorgi and Lionello, 2008; Peleg et al., 2015). For the Eastern Mediterranean, Kuglitsch et al. (2010) found that the duration (number) of heat waves in the region has increased ~eight (six) fold from 1960 to 2010. Regarding future projections, Lelieveld et al. (2014) provided evidence that the number of very hot days (daytime maximum temperature > 35 °C) in the coastal Levant may increase by more than two months until the end of the 21st century, while Zittis et al. (2016) found that the Eastern Mediterranean could be exposed to heat waves with amplitudes increased by up to 6 °C–10 °C and durations of up to 40 days. These changes occur in a region characterized by socioeconomic vulnerability and a fast-growing population (Cramer et al., 2018). Moreover, the high degree of urbanization in the region can aggravate the effects of heat waves through the urban heat island effect (Li and Bou-Zeid, 2013; Ward et al., 2016).

Although the Eastern Mediterranean's summer season is characterized by persistent synoptic conditions leading to high temperatures with relatively small inter-diurnal variability, comparatively cool weather or particularly high temperatures are no exception (Saaroni et al., 2003; Harpaz et al., 2014). The Persian Trough synoptic system governs over 80 % of July and August days at lower levels (Bitan and Saaroni, 1992; Alpert et al., 2004b; Ziv et al., 2004). It induces the north-westerly Etesian winds, bringing relatively cool and moist air from Eastern Europe and the Mediterranean Sea (Bitan and Saaroni, 1992; Ziv et al., 2004; Saaroni et al., 2017). The low-level cool advection and mid/upper-level subsidence induce a permanent inversion layer in the coastal areas, enhancing heat stress by trapping moisture below it (Ziv and Saaroni, 2011; Saaroni et al., 2017). Saaroni et al. (2017) proposed an environment-to-climate approach based on the so-called Climatic Stress Index (CSI) to improve earlier synoptic classifications of summer conditions in the region.

To characterize the persistence of heat waves, we use a recent approach grounded in dynamical systems theory. This perspective enables us to quantify the persistence of atmospheric states in phase space (Faranda et al., 2017). Indeed, Hochman et al. (2019, 2021) showed that the Persian Trough exhibits an exceptionally high persistence relative to other regional weather types and that heat days are, on average, more persistent than cooler days in summer.

Only a handful of studies have explored the effects of heat stress on mortality in the region, focusing mainly on Cyprus or big cities such as Tel-Aviv (Peretz et al., 2011; Leone et al., 2013; Heaviside et al., 2016). Moreover, the quantification of the impact of climate change and estimation of future death tolls attributable to heat has rarely been conducted for the region (Heaviside et al., 2016; Kendrovski et al., 2017; Ahmadalipour and Moradkhani, 2018).

Our study aims to provide detailed projections of heat wave frequency, duration, intensity, and dynamics in the Eastern Mediterranean. In addition, we investigate the heat-mortality relationship in Israel and provide an estimate of future excess mortality associated with increased heat stress.

2. Data

For evaluation of the model simulations and linking heat waves to mortality, we use daily values from 1976 to 2018 at a $0.25^\circ \times 0.25^\circ$ regular grid from the 5th generation of the European Centre for Medium-range Weather Forecasting (ECMWF) Reanalysis (ERA5; Hersbach et al., 2020). Extracted variables include temperature at 2 m, 1000 hPa, and 850 hPa, as well as surface and sea level pressure. Depending on the availability of the datasets to validate, different periods are used, namely 1976–2005 for model evaluation and 2000–2018 for health impact analysis.

For the projections, we utilize regional daily model data from the Coordinated Regional Downscaling Experiment (CORDEX), an initiative of the World Climate Research Programme (<https://cordex.org/>; Giorgi and Gutowski, 2015). We focus on data from the Middle East and North Africa region (MENA-CORDEX; <http://mena-cordex.cyi.ac.cy/>), which, compared to EURO- and Med-CORDEX captures the key regional weather types (Alpert et al., 2004a; Zittis et al., 2021). Here, we apply daily data from the Rossby Centre regional atmospheric model (RCA4; Strandberg et al., 2014; Samuelsson et al., 2015) forced by three different global circulation models at grid-spacing ranging from $0.22^\circ \times 0.22^\circ$ to $0.44^\circ \times 0.44^\circ$. The latter were driven under Representative Concentration Pathways (RCPs), which comprise a commonly used representative-of-literature set of four greenhouse gas concentration trajectories for the 2005–2100 simulation period associated with a corresponding change in radiative forcing, respective (global) temperature (van Vuuren et al., 2011). We consider three Representative Concentration Pathways (RCP) with an additional radiative forcing of 2.6, 4.5, and 8.5 W/m² at the end of the century compared to pre-industrial levels, representing the lowest, intermediate, and highest greenhouse gas concentration trajectories (RCP2.6, RCP4.5, and RCP8.5; Table 1). This corresponds to all publicly available regional model simulations containing the necessary variables for computing the CSI. Extracted variables include temperature at 2 m and 850 hPa as well as surface and sea level pressure. The model data is then interpolated to a standard $0.25^\circ \times 0.25^\circ$ grid to match the ERA5 data.

Finally, to quantify the heat-mortality relationship, we employ data from the Israel Central Bureau of statistics on the daily death toll, monthly average total population, and annual average population by age for Israel from 2000 to 2018.

3. Methods

3.1. Computation of the Climatic Stress Index (CSI) and heat wave indices

The Climatic Stress Index (CSI) is based on the Discomfort Index (Thom, 1959; Sohar et al., 1978) and the height of the marine inversion base. This environment-to-climate approach to classifying summer days provides valuable information on local weather conditions (Saaroni et al., 2017, 2018). We chose the CSI for studying heat waves as it combines temperature, humidity, and circulation (Saaroni et al., 2017, 2018). These variables are important factors for human well-being (Armstrong, 2006; Epstein and

Table 1

Specifying model data by global driving model, spatial resolution, and Representative Concentration Pathway (RCP) scenario. Historical (Hist) forcing until 2005, from 2005 to 2100 RCP forcing.

Driving model	Resolution	Scenario
EC-Earth	$0.44^\circ \times 0.44^\circ$	Hist, RCP 2.6/4.5/8.5
	$0.22^\circ \times 0.22^\circ$	Hist, RCP 2.6/4.5/8.5
GFDL-ESM2M	$0.44^\circ \times 0.44^\circ$	Hist, RCP 2.6/4.5/8.5
	$0.22^\circ \times 0.22^\circ$	Hist, RCP 2.6/4.5/8.5
CNRM-CM5	$0.44^\circ \times 0.44^\circ$	Hist, RCP 2.6/4.5/8.5

Moran, 2006; Ahmadalipour and Moradkhani, 2018), while at the same time, its approximation formula requires variables commonly included in model outputs. The CSI is calculated as follows:

$$CSI = 92.78 + 0.638T_{1000-850} - 0.178\Delta p - 0.108p_{Iran}. \quad (1)$$

Here, $T_{1000-850}$ is the mean between air temperature at 1000 hPa and 850 hPa averaged over $[31^{\circ}\text{N}-34^{\circ}\text{N}; 33^{\circ}\text{E}-37^{\circ}\text{E}]$. It represents the regional lower-level ambient temperature over the Levant. Δp is the mean sea level pressure averaged over West Egypt $[24^{\circ}\text{N}-29^{\circ}\text{N}; 21^{\circ}\text{E}-29^{\circ}\text{E}]$ minus the mean sea level pressure averaged over the South Caucasus $[36^{\circ}\text{N}-44^{\circ}\text{N}; 42^{\circ}\text{E}-54^{\circ}\text{E}]$. It is a proxy for the intensity of the Etesian Winds. p_{Iran} is the

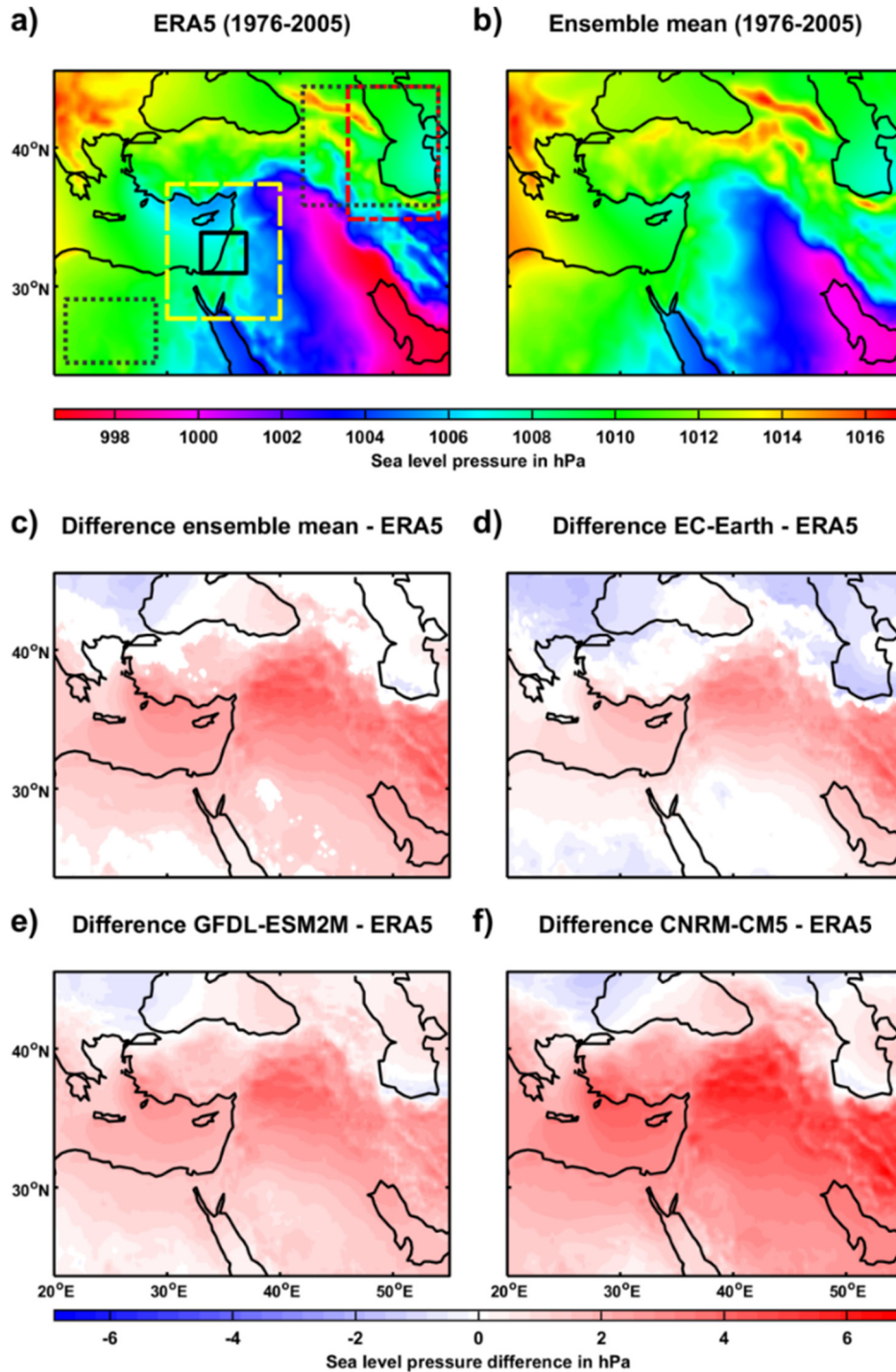


Fig. 1. Median sea level pressure map for the historical period (1976–2005) of ERA5 (a), the model ensemble mean (b), the difference between the multimodel ensemble mean (c) EC-Earth (d) GFDL-ESM2M (e) and CNRM-CM5 (f) compared to ERA5. Only significant differences according to the Wilcoxon-Ranksum test at the 5 % significance level are colored. Boxes in the upper left panel show Israel/Jordan (black line, $31^{\circ}\text{N}-34^{\circ}\text{N}; 33^{\circ}\text{E}-37^{\circ}\text{E}$), representing the regional lower-level ambient temperature ($T_{1000-850}$), West Egypt and South Caucasus (dotted grey line, $24^{\circ}\text{N}-29^{\circ}\text{N}; 21^{\circ}\text{E}-29^{\circ}\text{E}$ and $36^{\circ}\text{N}-44^{\circ}\text{N}; 42^{\circ}\text{E}-54^{\circ}\text{E}$), as a proxy of the intensity of the Etesian winds (Δp) and North Iran (red dashed-dotted line, $35^{\circ}\text{N}-44^{\circ}\text{N}; 46^{\circ}\text{E}-54^{\circ}\text{E}$) to quantify the depth of the Persian Trough (p_{Iran}). All of the above are used for computing the CSI. Shown as well is the region for which inverse persistence (θ) of the 2-meter temperature field is calculated (yellow dashed line, $27.5^{\circ}\text{N}-37.5^{\circ}\text{N}; 30^{\circ}\text{E}-40^{\circ}\text{E}$). (For interpretation of the references to color in this figure legend, the reader is referred to the web version of this article.)

mean sea level pressure averaged over North Iran [35°N–44°N; 46°E–54°E], representing the depth of the Persian Trough. The application period of the CSI encompasses July and August when the Persian Trough and the Etesian winds are the dominant synoptic patterns (Alpert et al., 2004b; Hochman et al., 2021). The regions used for the computation of CSI are shown in Fig. 1 a.

We approximate the 1000 hPa temperature, as it is unavailable for the model runs. The correlation between the 1000 hPa temperature and its approximation is $R = 0.99$ for ERA5, see Suppl. Text S1. Further, the daily CSI distributions of the model are bias-corrected via the ‘(EquiDistant)

Cumulative Distribution Function (matching)’ method for the historical (projection) periods (Li et al., 2010; Wang and Chen, 2014).

We define a heat day as a day on which the CSI exceeds the 90th percentile (Hochman et al., 2021), henceforth the Heat Day Threshold (HDT) of the historical (1976–2005) ERA5 daily CSI distribution. A heat wave consists of at least three consecutive heat days (Perkins and Alexander, 2013; Chen et al., 2015; Zittis et al., 2021). Indeed, the HDT proves to be a reasonable choice when investigating the CSI-mortality relationship, as there is a sharp increase in correlation around the 90th percentile of the CSI, especially in the elderly population (Fig. 2).

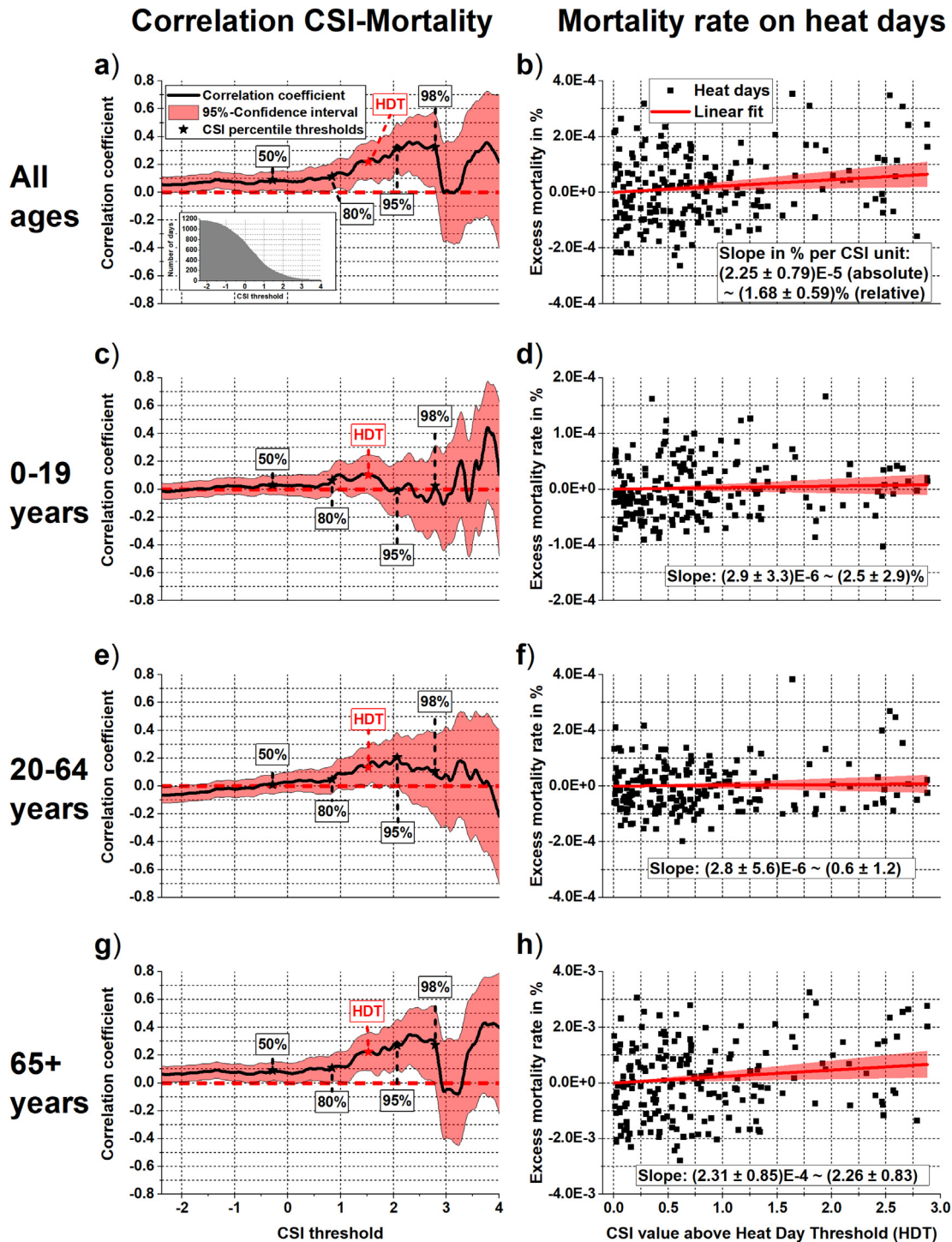


Fig. 2. CSI vs. mortality relationship for all ages (a, b) 0–19 years (c, d) 20–64 years (e, f) and 65+ years (g, h). The left panels show the correlation between daily mortality and CSI when only considering days above a CSI threshold. The right panels show CSI-mortality diagrams with linear fits.

We introduce several heat stress indices to evaluate heat stress conditions mainly based on the framework constructed by Perkins et al. (2012) and Perkins and Alexander (2013):

- **Average Climatic Stress (ACS):** Median daily CSI value assesses the average heat stress on a summer day.
- **Heat Day Frequency (HDF):** Mean number of heat days per summer assesses the probability of days exacerbating high heat stress.
- **Heat Wave Frequency (HWF):** Mean number of heat waves per summer assesses the probability of prolonged events of high heat stress.
- **Heat Wave Duration (HWDu):** Mean duration of a heat wave quantifies the average length of a prolonged heat stress episode.
- **Average Heat Wave Day Climatic Stress (AHWDCS):** Median daily CSI value on heat wave days evaluates the average heat stress during episodes of high heat stress.
- **Heat Wave Severity (HWS):** Median heat wave severity. The severity of a heat wave is the sum of all daily CSI values minus the 90th percentile of CSI values. It measures the accumulated excess heat stress during a heat wave, comparable to the Excess Heat Factor (EHF) introduced by Nairn and Fawcett (2014).

To assess how changes in the variables, i.e., low-level temperature and circulation changes related to the sea level pressure variables, contribute to the CSI increase, we exploit the multiple linear form of Eq. (1). We estimate the linear contribution C_x of a variable x by its average change weighted with its prefactor (see Eq. (1)) divided by the average CSI change:

$$C_x = w_x \cdot \frac{\langle x_{proj} \rangle - \langle x_{hist} \rangle}{\langle CSI_{proj} \rangle - \langle CSI_{hist} \rangle}, \quad (2)$$

where *proj* and *hist* represent the projected and historical distribution, respectively. Note that this estimate neglects indirect effects such as interaction among the variables and can therefore not address the question of causal attribution of the individual variables (Trenberth et al., 2015).

3.2. Computation of persistence

To assess the persistence of heat waves in a changing climate, we use recent developments in the theory of dynamical systems, which enable the computation of such instantaneous properties of 2-dimensional atmospheric states (Lucarini et al., 2016; Faranda et al., 2017). We compute the quantity $\theta(\zeta)$, which measures the inverse persistence of a state ζ in phase space. More details on this can be found in Lucarini et al. (2016), Faranda et al. (2017), and Hochman et al. (2021).

Here, we apply this method to compute the persistence of the daily latitude-longitude 2 m temperature fields over the region (yellow box in Fig. 1 a). This domain [27.5°N–37.5°N; 30°E–40°E] is consistent with previous studies (Hochman et al., 2021, 2022), which demonstrated the relatively low sensitivity of θ to domain size and location (Hochman et al., 2022). We consider anomalies from the seasonal cycle, computed by averaging θ for a given date from 1976 to 2005. Values below zero indicate a more persistent behavior than expected for that date in summer compared to the long-term mean and vice versa.

We then computed θ for the climate projections. We assume that the persistence of a given state does not change much in a warmer world, but rather the overall probability of reaching that state might be shifted.

3.3. Quantification of heat-related mortality

We describe the relationship between CSI and mortality both qualitatively and quantitatively. We test for a threshold above which the mortality increases with the CSI (Armstrong, 2006; Baccini et al., 2008). We do this by correlating CSI and daily mortality rates above different CSI thresholds. Mortality rates are computed by dividing the daily death count by the corresponding population group count. We find a threshold at ~90th CSI percentile, most pronounced for the elderly and total population, justifying our

definition of heat day threshold at the 90th percentile (Fig. 2 a, c, e, g). Above this threshold, the correlation coefficient is significantly different from zero for the total population and the elderly (65+ years). Note that the correlation between mortality and CSI among the different age groups is highest among the elderly.

To quantify the mortality behavior, we assume a simple linear model, hypothesizing that the mortality rate increases linearly with the daily CSI value above the Heat Day Threshold. Further, we assume some lag effect of heat stress. We assume the impact of a heat day to decrease linearly with time. Mathematically the mortality rate $\lambda(t)$ on a heat day t is given in this model by:

$$\begin{aligned} \lambda(t) &= a + b \cdot \frac{3 \cdot eCSI(t) + 2 \cdot eCSI(t-1) + 1 \cdot CSI(t-2)}{6} \\ &= a + b \sum_{i=0}^{3-i} \frac{3-i}{6} eCSI(t-i), \end{aligned} \quad (3)$$

where $eCSI(t) = CSI(t) - \text{HDT}$.

3.4. Statistical inference

We compute the ensemble mean by averaging the driving model-specific values. If available, the latter is computed by averaging the values from both spatial resolutions. Significance on the 5 %-level is tested using the Wilcoxon rank sum test (for median sea level pressure maps) or bootstrapping with 10,000 realizations. We use two-sided tests for the historical period and a one-sided test for the projections.

4. Results

4.1. Evaluation of MENA-CORDEX model simulations

We first evaluate the model's ability to simulate the variables constituting the CSI. The median sea level pressure pattern over the Eastern Mediterranean is well captured (cf. Fig. 1 a to b). All model runs show an overestimation, mostly over mountainous regions such as the Zagros Mountains in Iraq or the East Anatolian Mountain ranges, as well as over parts of the Eastern Mediterranean Sea (Fig. 1 c–f). There is a slight underestimation over the Romanian Plains and the Western Black Sea (Fig. 1 c–f). Most importantly, the regions used for the CSI calculation (see Fig. 1 a), including South Caucasus, the Caspian Sea as well as East Libya/West Egypt, are resolved well with almost no (significant) bias in the models (Fig. 1 c–f). Accordingly, the temperature at 850 hPa and 1000 hPa distributions are reproduced well (see Fig. 3 a, b).

We evaluate the different heat stress metrics following the bias correction of the CSI model distributions. Fig. 4 shows that the individual model runs capture the range of ERA5 values. All heat stress metrics for the model mean (Supplementary Table S1) and each model run alone (not shown) are not significantly different from the ERA5 values.

Moreover, we quantify the persistence in phase space of the 2-meter temperature field over the broader region of the Levant, which we use as a proxy for atmospheric heat wave conditions. As in Hochman et al. (2021), heat days are marked by a higher persistence than non-heat days (Fig. 5). Indeed, CSI correlates to the 2-meter temperature field persistence, qualitatively and quantitatively captured by the model simulations. This indicates a less persistent behavior below some threshold and an increasing persistence with CSI above that threshold. We conclude that the outputs of the MENA-CORDEX simulations provide a good representation of the metrics compared to ERA5 and therefore use them next for future projections.

4.2. Future projections of heat wave characteristics

The corresponding heat wave characteristics projections for future decades are shown in Fig. 6 and Supplementary Tables S2 and S3. We find a significant increase in all heat metrics under all scenarios for both future

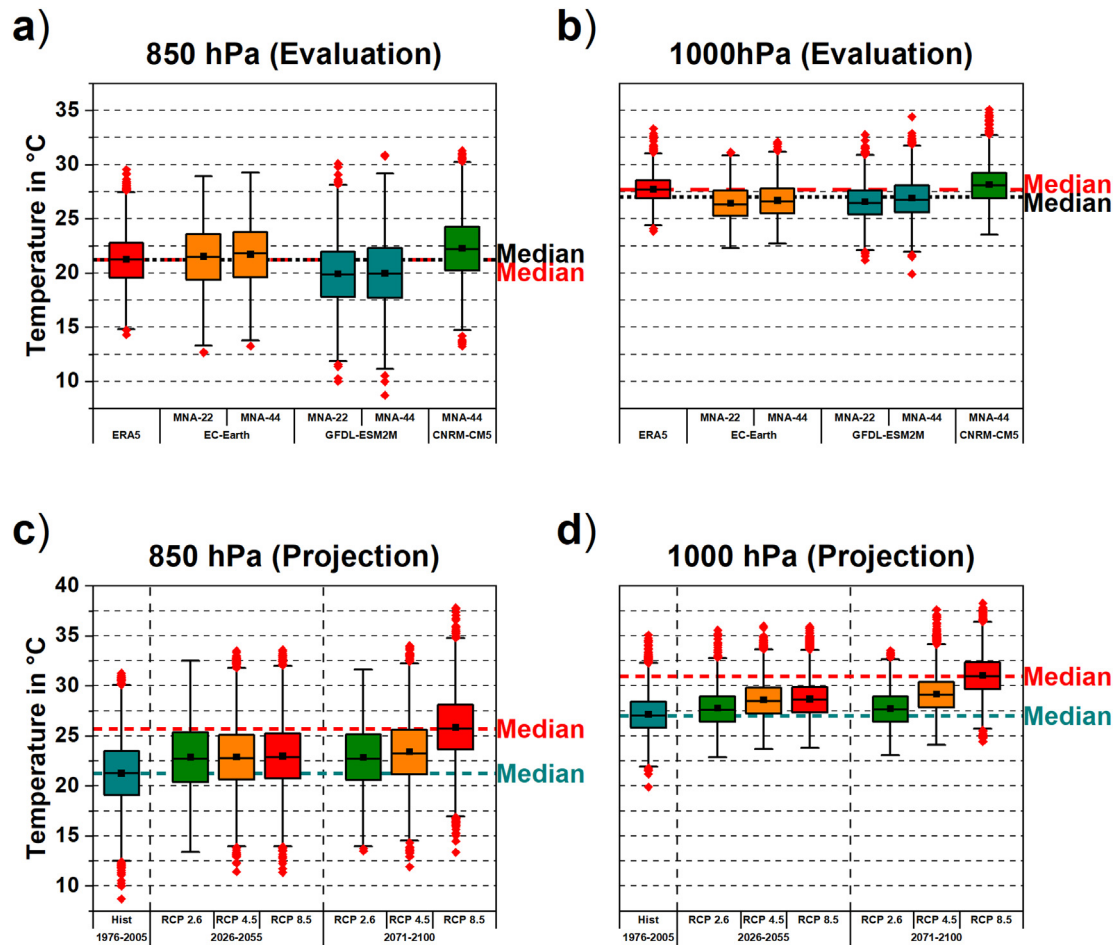


Fig. 3. Boxplots for ERA5 and the different model simulations showing the distribution of the historical temperature in the high summer season (July and August) over Israel (black rectangle in Fig. 1 a) at 850 hPa (a) and 1000 hPa (b). (c, d) same as (a, b) but for the multimodel ensemble mean projections and for the periods 1976–2005, 2026–2055, and 2071–2100 under three RCP scenarios (RCP2.6, RCP4.5, and RCP8.5). The median temperature for ERA5 and the model mean are blue, and red dashed lines, respectively (a, b). Similarly, the 1976–2005 model median temperature is a blue and red dashed line for 2071–2100 under RCP 8.5 (c, d). (For interpretation of the references to color in this figure legend, the reader is referred to the web version of this article.)

periods compared to the evaluation period. The distributions show a clear pattern marked by a similar intensification of heat stress conditions towards the near future (2026–2055), while for the end of the century (2071–2100), the RCP 2.6 scenario shows a slight decline as may be expected for this pathway. The RCP 4.5 and RCP 8.5 scenarios show an increase compared to mid-century, which is more robust in the RCP 8.5 scenario. Considering the changes in CSI as an example: Towards mid-century, the average CSI increases by about 40 % to 80 % of the CSI standard deviation, while towards end-of-century, compared to mid-century, it stays approximately constant for RCP 2.6, increases another 20 % to 30 % for RCP 4.5, and additional 130 % for RCP 8.5 (Fig. 6 a and Supplementary Tables S2 and S3).

We highlight that the heat day frequency is projected to increase by ~2–8 times the base value at the end of the century, depending on the scenario. This will lead to summers consisting solely of heat days at the end of the century under RCP 8.5. In addition, the heat wave frequency will increase from 1 to 2 heat waves per summer in the near future and three at the end of the century under RCP 4.5 and RCP 8.5, respectively. The average heat wave duration is projected to increase by 30–200 %, depending on the scenario. Finally, the average heat wave severity may increase by ~3.5 times under RCP 8.5 at the end of the century.

Next, we estimate the direct contribution of low-level temperature and circulation changes to the increases in CSI values. We find that changes in low-level temperature contribute ~90–95 % to the change in CSI compared to only ~5–10 % change associated with sea level pressure, i.e., circulation. This is found in the average CSI change and the average CSI change within

the upper 10 %-tail of the corresponding distributions. It encompasses temperature increases of over 2 K at the end of the century for both 850 hPa and 1000 hPa. The regions on which CSI is computed show little change in sea level pressure (Fig. 7). We note, however, that the median sea level pressure increases over mountainous regions like Anatolia and Greece while it decreases over the Mediterranean Sea and the Levant, which might lead to an intensification of the Etesian winds in the future (Anagnostopoulou et al., 2014; Dafka et al., 2019).

We provide evidence that future heat day temperature patterns and atmospheric heat wave conditions might manifest an even more persistent behavior than their historical counterparts. Indeed, the persistence of heat days increases (decrease of θ), indicating the influence of elevated greenhouse gas concentrations on the persistence of heat days (Fig. 8 and Supplementary Fig. S1). The CSI and persistence anomaly are highly correlated ($R \approx 0.8$), hinting at a synoptic mechanism enhancing the persistence of high heat stress conditions.

4.3. Heat-mortality relationship and estimate of future heat-related mortality

We apply a simple linear model (Sect. 3.3) to describe the CSI-mortality relationship. We find that the highest absolute increase in mortality rate is most prominent for the elderly. Indeed, the relative increase in mortality rate per unit CSI corresponds to $2.5 \% \pm 2.9 \%$ for young people, $0.6 \% \pm 1.2 \%$ for adults, and $2.3 \% \pm 0.8 \%$ for the elderly (Fig. 2 b, d, f, h). Assuming causality, we estimate that the historical heat stress conditions have led

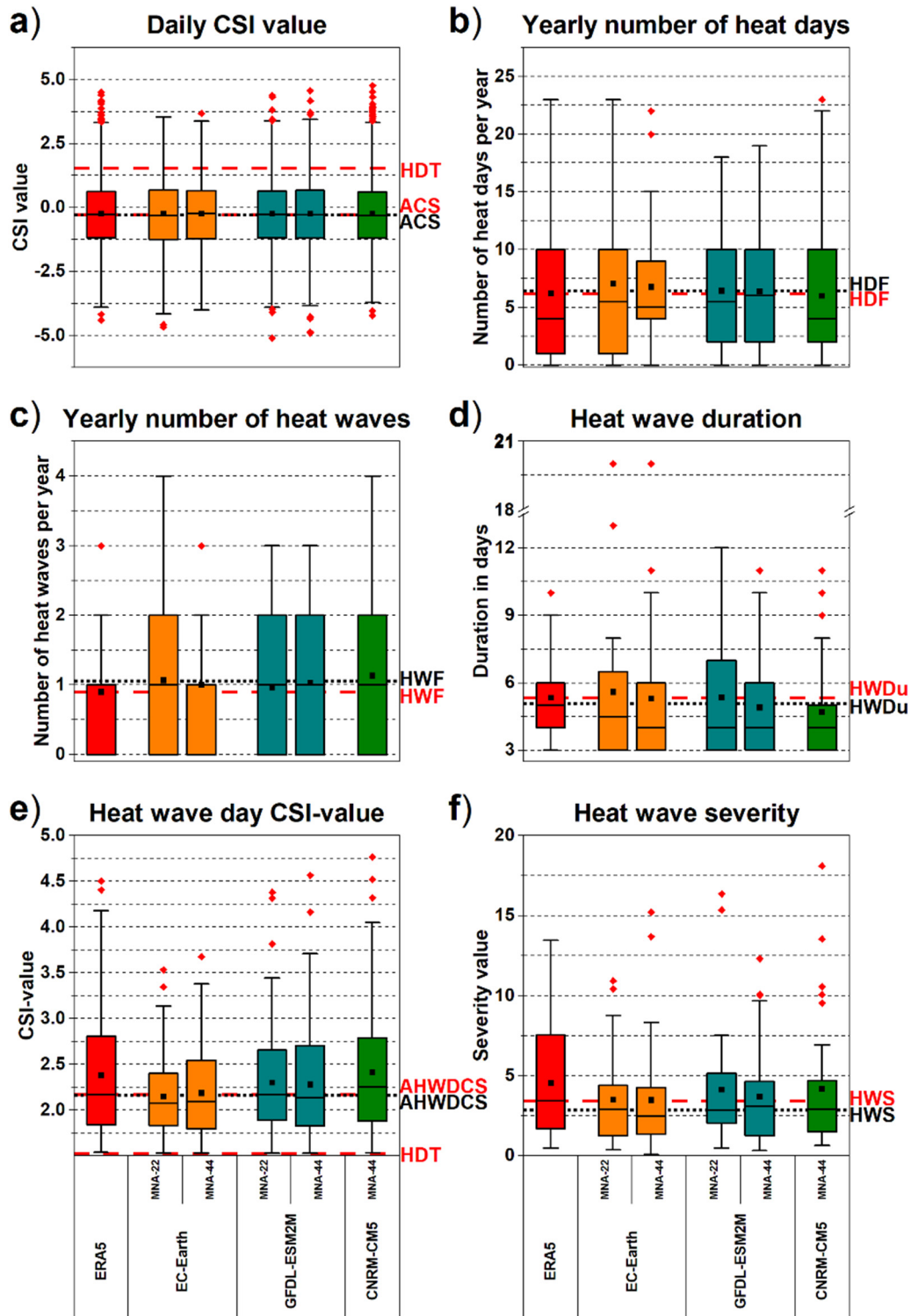


Fig. 4. Boxplots of the distributions used for computing the heat stress metrics for ERA5 and regional climate model for the historical period (1976–2005). The indices considered are Average Climatic Stress (ACS) in CSI units (a), Heat Days Frequency (HDF) in days per year (b), Heat Wave Frequency (HWF) in number of heat waves per year (c), Heat Wave Duration (HWDu) in days (d), Average Heat Wave Day Climatic Stress (AHWDCS) in CSI units (e), Heat Wave Severity (HWS) in CSI units (f). Heat stress metric values of ERA5 (model mean) are indicated by the red dashed line (black dotted line). Red diamonds represent outliers in the diagram. Mean (median) values are represented by black squares (black lines) inside the box plots. (For interpretation of the references to color in this figure legend, the reader is referred to the web version of this article.)

to $\sim 30 \pm 10$ additional deaths per summer, which is about 0.4 % of the total death count. Assuming the linear model holds for CSI values outside the historical range and no change in the demographic structure or CSI-mortality relationship, we can estimate the number of excess deaths for

the climate projections. For 2026–2055, about 0.70 ± 0.30 more people per summer per 100,000 inhabitants might die due to increasing heat stress in Israel, increasing the attribution of heat-related deaths to about 1.2 %. At the end of the century, these numbers change to 0.55 ± 0.20 (~1 %),

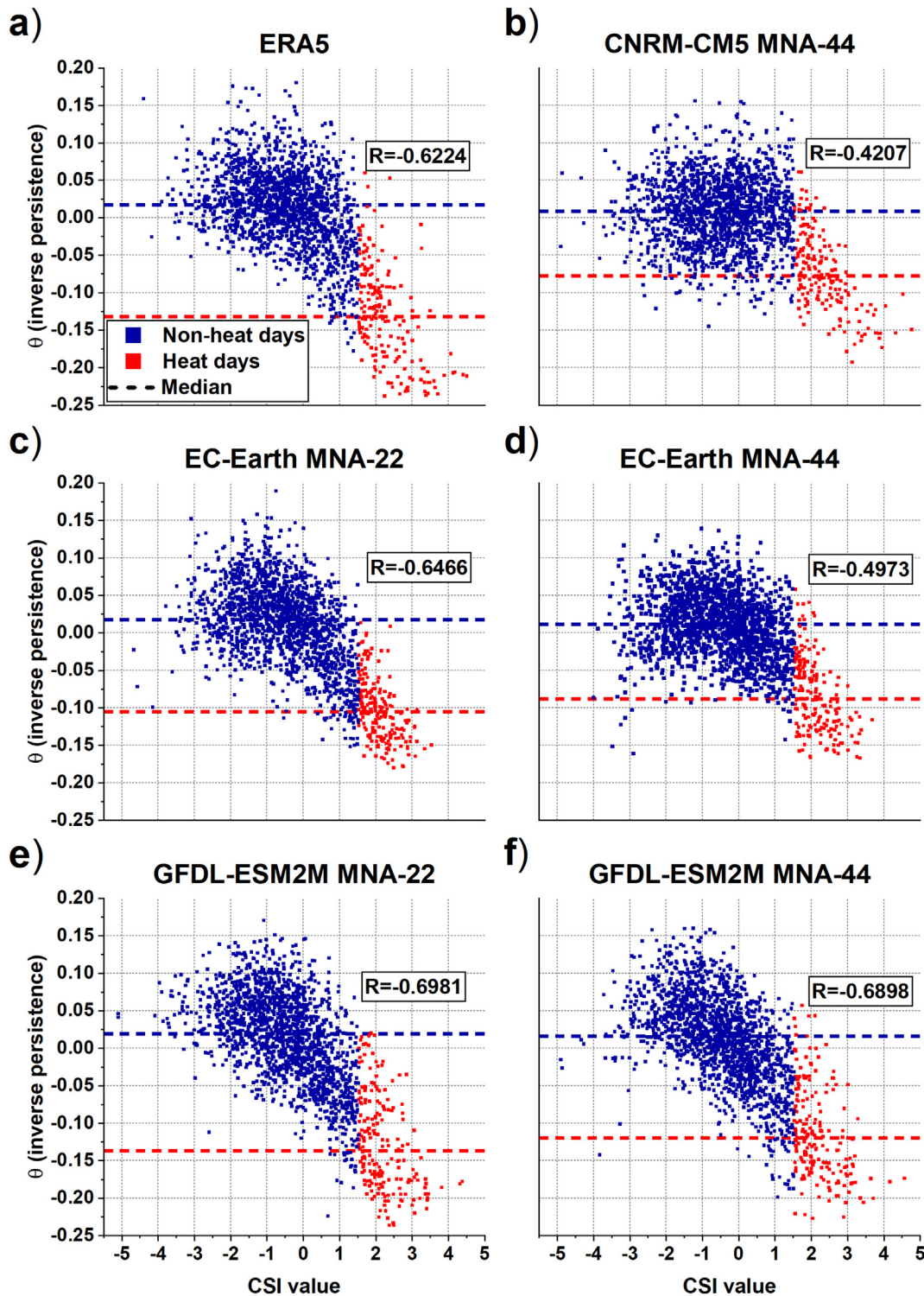


Fig. 5. Climatic Stress Index (CSI) vs. inverse persistence (θ) anomalies computed on 2 m temperature for the region in Fig. 1 a (see Sect. 3.2). Diagrams for ERA5 (a) and the regional model simulations including CNRM-CM5 MNA-44 (b) EC-Earth MNA-22 (c) and MNA-44 (d), GFDL-ESM2M MNA-22 (e) and MNA-44 (f).

0.95 ± 0.35 (~1.5 %), and 3.00 ± 1.05 (~4 %) under RCP 2.6, 4.5, and 8.5, respectively. Assuming a constant population of about 10 million, this would correspond to ~300 more excess deaths due to heat stress at the end of the century under RCP 8.5. It should be noted that we consider a rather conservative linear model for the dependence of mortality on CSI values. However, the increase may show nonlinear (exponential) effects, resulting in larger excess mortality estimates than ours.

5. Discussion and conclusions

Our analysis has shown that the characteristics of heat waves for the Eastern Mediterranean increase in frequency, intensity, and duration in a warmer climate. Our results are in line with studies providing evidence of an increase in heat stress in the region (Lelieveld et al., 2016; Zittis et al., 2021). Moreover, there is a consensus that the duration, magnitude, and

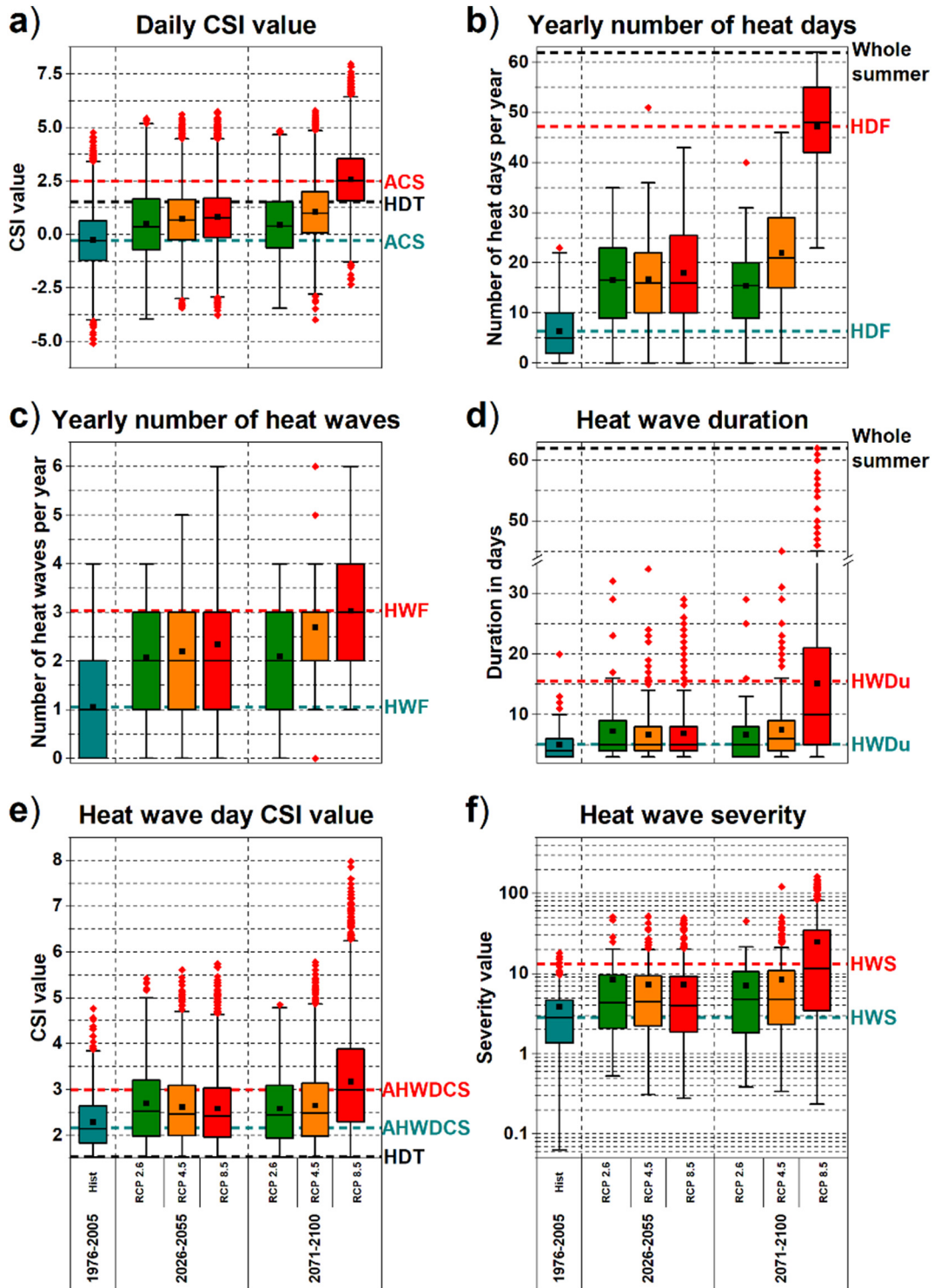


Fig. 6. Same as Fig. 4, but for different RCP scenarios (RCP2.6, RCP4.5, and RCP8.5) and three different periods (1976–2005, 2026–2055, and 2071–2100). Heat stress metric values of the historical model mean (RCP8.5 at the end of the century) are indicated in a blue dashed line (red dotted line). The black dashed line indicates the number of summer days considered, i.e., July and August. (For interpretation of the references to color in this figure legend, the reader is referred to the web version of this article.)

frequency of heat waves will increase. This study adds to the literature by comprehensively examining projected heat wave characteristics using a region-specific heat stress index combining temperature, humidity, circulation, and related measures. Though it is difficult to compare directly, our projected proportion of heat days under RCP 8.5 (1976–2005: 10%–11%, 2026–2055: 27%–31%; 2071–2100: 73%–82%) compares well to that of warm days over the whole year in the MENA region (1986–2005: ~15%; 2046–2065: 46% ± 9% RCP 8.5; 2081–2100:

67% ± 9% RCP 8.5), as found by Lelieveld et al. (2016). Our results for average heat wave duration under RCP 8.5 (1976–2005: 4.7–5.6 days; 2026–2055: 6.5–7.1 days; 2071–2100: 12.1–19.3 days) fall in the range of Zittis et al.'s (2021) findings. Finally, Zittis et al. (2016, 2021) and Driouech et al. (2020) report heat waves of an unprecedented duration of up to several months, which aligns with our evidence that summers may consist of a single long heat wave in the future. Although direct comparison is difficult, the projected increase in the persistence of heat days

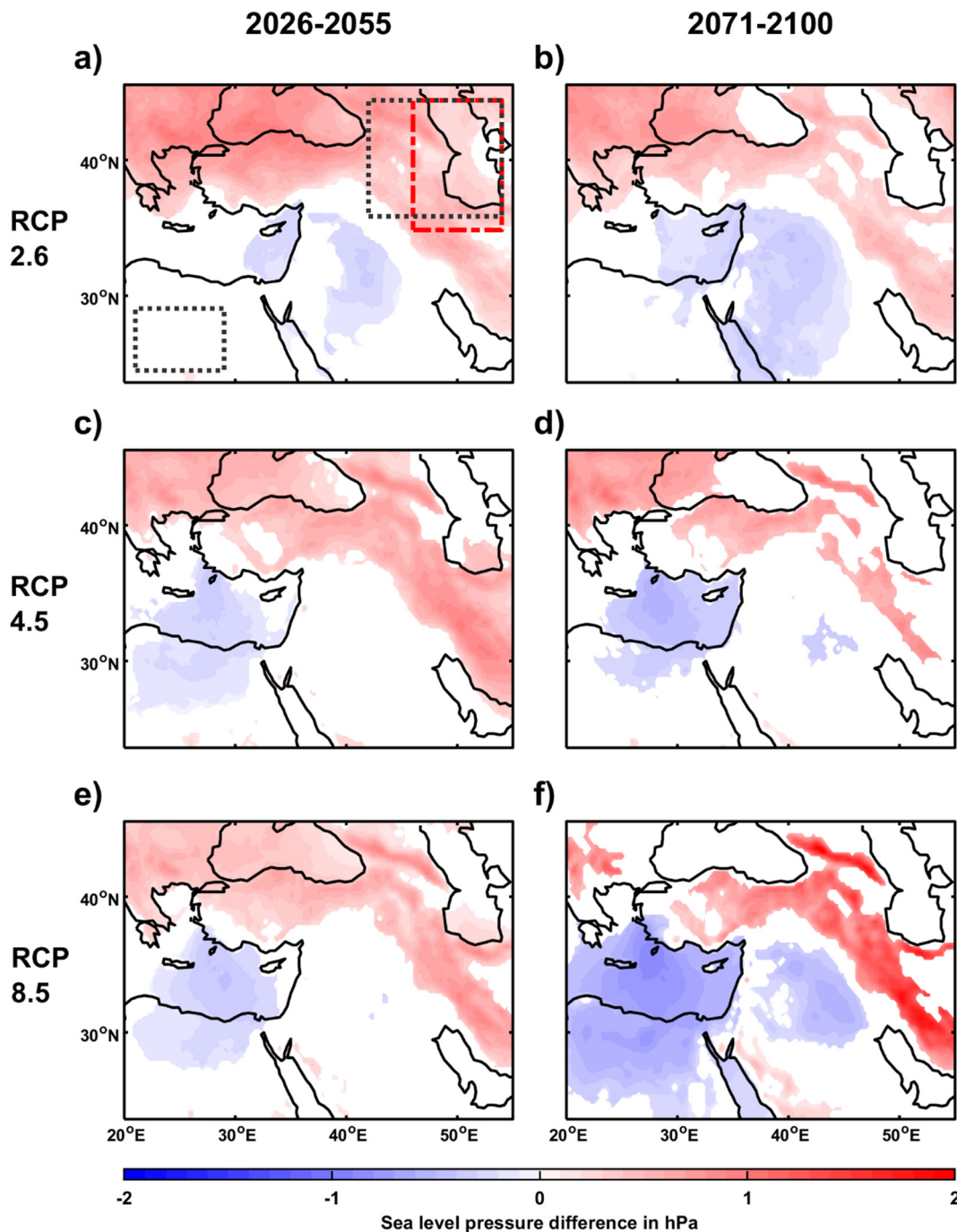


Fig. 7. Sea level pressure difference maps of the multimodel ensemble mean under three RCP scenarios (RCP2.6, RCP4.5, and RCP8.5) for mid-century (2026–2055) and end century (2071–2100) with respect to 1976–2005. Only significant differences (for the medians) using the Wilcoxon-Ranksum test at the 5 % significance level are colored.

qualitatively agrees with [Pfleiderer et al. \(2019\)](#), who provided evidence that warm summer weather become more persistent in a 2 °C warmer world. As the persistence of heat days is a main driver of heat wave duration, it is essential that future research explores the causes behind this increase in heat persistence. Possible explanations may include a shallowing of the Persian trough, combined with the North Africa thermal low ([Lelieveld et al., 2016](#); [Zittis et al., 2021](#)) and the connection of heat wave persistence to soil moisture ([Perkins, 2015](#)) in a drier future climate ([Hochman et al., 2018](#)). Overall, our results demonstrate how drastically increasing greenhouse gas concentrations may aggravate the heat stress conditions in the Eastern Mediterranean.

Here, we provide the first estimates for Israel's heat-mortality relationship and future projections, which are essential for developing

appropriate public health strategies in response to heat stress. We find that heat-related mortality effects are more significant for the elderly (65+ years; +2.3 % ± 0.8 % increased mortality rate per unit CSI) than for the total population (+1.7 % ± 0.6 %; [Åström et al., 2011](#); [Chen et al., 2015](#)). These values fall in range with results from [Peretz et al. \(2011\)](#) and [Leone et al. \(2013\)](#) for the Tel Aviv district. Compared to mortality projections for the nearby island of Cyprus, [Heaviside et al. \(2016\)](#) have estimated a 10-fold higher historical heat-related mortality, and [Kendrovski et al. \(2017\)](#) arrived at a 5-fold higher historical attribution of heat-related mortality. This could be partially associated with different demographics or analysis methods. However, our estimates corresponding to ~4- and ~10-fold the historical heat-related mortality under RCP 4.5, and RCP 8.5, respectively, agree with the

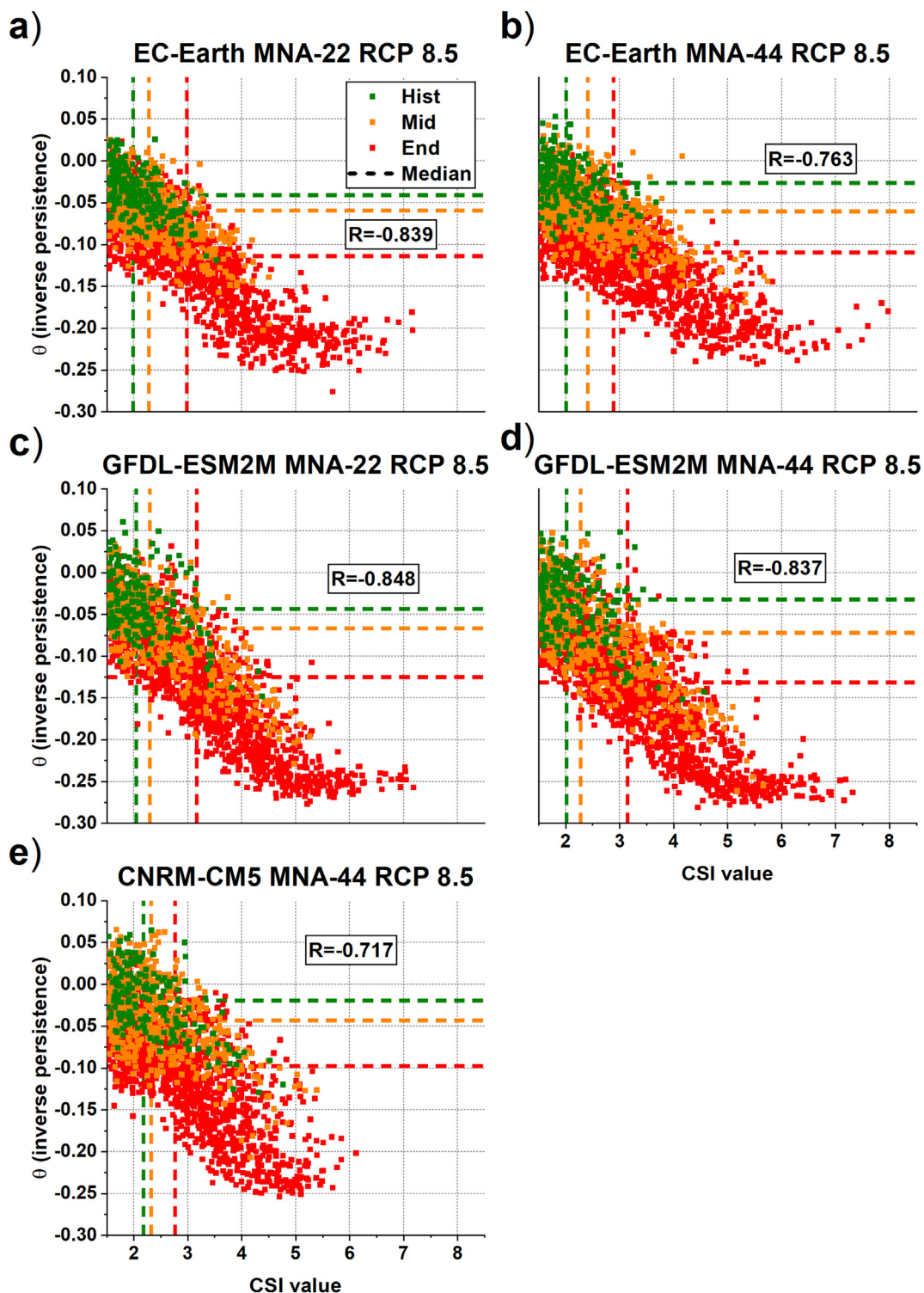


Fig. 8. Same as Fig. 5, but for model projections under the RCP8.5 scenario. The considered models are EC-Earth MNA-22 (a) and MNA-44 (b) GFDL-ESM2M MNA-22 (c) and MNA-44 (d), and CNRM-CM5 MNA-44 (e). The considered periods are 1976–2005 (Hist), 2026–2055 (Mid), and 2071–2100 (End). Dashed lines represent the historical (green), mid-century (orange), and end-century (red) median persistence anomaly of heat days. (For interpretation of the references to color in this figure legend, the reader is referred to the web version of this article.)

estimates by Heaviside et al. (2016), Kendrovski et al. (2017) and Ahmadalipour and Moradkhani (2018).

Our heat wave projections are subject to some uncertainties that arise from the global and regional climate models, the initial conditions of the simulations, and the downscaling domain (Giorgi and Gutowski, 2015; Syed et al., 2019). These uncertainties can be assessed using a larger

ensemble of simulations currently unavailable for the MENA-CORDEX area and considering different resolutions and downscaling domains. Our estimate of projected mortality associated with heat stress is subject to uncertainties due to the natural variability of mortality, potential confounders, and conservative assumptions regarding the heat-mortality relationship. It is desirable to explore these uncertainties with more

comprehensive datasets, currently not publicly available, and by relaxing the conservative assumptions, e.g. allowing for a more complex functional form of the heat-mortality relationship, in future research.

We conclude that in a warming world, heat waves pose an increasing threat to society in the vulnerable Eastern Mediterranean. We emphasize that true interdisciplinary regional collaborations are required to develop adequate public health adaptation to extreme weather events in a changing climate.

CRedit authorship contribution statement

AH developed the original idea for the paper and supervised the work. MW, AH, and JGP developed the concept. MW performed the data analysis and prepared the figures. A first draft was created by MW with support from AH. All authors contributed with discussions and revisions.

Data availability

ERA5 data was retrieved from the Copernicus Climate Change Service Climate Data Store (<https://cds.climate.copernicus.eu/#/search?text=>). CORDEX data was acquired from the Earth System Grid Federation – Commodity Governance (ESGF-CoG) data node (<https://esg-dn1.nsc.liu.se/projects/esgf-liu/>). Mortality and population datasets were extracted from the Israel Central Bureau of Statistics website (<https://www.cbs.gov.il>).

Declaration of competing interest

The authors declare no competing interests.

Acknowledgments

AH acknowledges the Hebrew University for providing technical support. JGP thanks the AXA Research Fund for its support.

Funding

The German Helmholtz Association “Changing Earth” program in the case of AH and MW has supported this research. The Ministry of Science, Innovation, and Technology of Israel partly funded the contribution of AH. The AXA Research Fund partly supported JGP.

Code availability

Code for computation of persistence (θ ; Faranda et al., 2017) is freely available at <https://de.mathworks.com/matlabcentral/fileexchange/95768-attractor-local-dimension-and-local-persistence-computation>.

Appendix A. Supplementary data

Supplementary data to this article can be found online at <https://doi.org/10.1016/j.scitotenv.2023.161883>.

References

Ahmadalipour, A., Moradkhani, H., 2018. Escalating heat-stress mortality risk due to global warming in the Middle East and North Africa (MENA). *Environ. Int.* 117, 215–225. <https://doi.org/10.1016/j.envint.2018.05.014>.

Alpert, P., Osetinsky, I., Ziv, B., Shafir, H., 2004a. A new seasons definition based on classified daily synoptic systems: an example for the eastern Mediterranean. *Int. J. Climatol.* 24, 1013–1021. <https://doi.org/10.1002/joc.1037>.

Alpert, P., Osetinsky, I., Ziv, B., Shafir, H., 2004a. Semi-objective classification for daily synoptic systems: application to the eastern Mediterranean climate change. *Int. J. Climatol.* 24, 1001–1011. <https://doi.org/10.1002/joc.1036>.

Anagnostopoulou, C., Zanis, P., Katragkou, E., Tegoulas, I., Tolika, K., 2014. Recent past and future patterns of the etesian winds based on regional scale climate model simulations. *Clim. Dyn.* 42, 1819–1836. <https://doi.org/10.1007/s00382-013-1936-0>.

Armstrong, B., 2006. Models for the relationship between ambient temperature and daily mortality. *Epidemiology* 17, 624–631. <https://doi.org/10.1097/01.ede.0000239732.50999.8f>.

Åström, D.O., Forsberg, B., Rocklöv, J., 2011. Heat wave impact on morbidity and mortality in the elderly population: a review of recent studies. *Maturitas* 69, 99–105. <https://doi.org/10.1016/j.maturitas.2011.03.008>.

Baccini, M., et al., 2008. Heat effects on mortality in 15 European cities. *Epidemiology* 19, 711–719. <https://doi.org/10.1097/ede.0b013e318176bfcd>.

Becker, F.N., Fink, A.H., Bissoli, P., Pinto, J.G., 2022. Towards a more comprehensive assessment of the intensity of historical European heat waves (1979–2019). *Atmos. Sci. Lett.* 23, e1120. <https://doi.org/10.1002/asl.1120>.

Belhadj Slimen, I., Najjar, T., Ghram, A., Abdrabba, M., 2016. Heat stress effects on livestock: molecular, cellular and metabolic aspects, a review. *J. Anim. Physiol. Anim. Nutr.* 100, 401–412. <https://doi.org/10.1111/jpn.12379>.

Bitan, A., Saaroni, H., 1992. The horizontal and vertical extension of the Persian Gulf pressure trough. *Int. J. Climatol.* 12, 733–747. <https://doi.org/10.1002/joc.3370120706>.

Chen, K., Bi, J., Chen, J., Chen, X., Huang, L., Zhou, L., 2015. Influence of heat wave definitions to the added effect of heat waves on daily mortality in Nanjing, China. *Sci. Total Environ.* 506–507, 18–25. <https://doi.org/10.1016/j.scitotenv.2014.10.092>.

Coumou, D., Rahmstorf, S., 2012. A decade of weather extremes. *Nat. Clim. Chang.* 2, 491–496. <https://doi.org/10.1038/nclimate1452>.

Cramer, W., et al., 2018. Climate change and interconnected risks to sustainable development in the Mediterranean. *Nat. Clim. Chang.* 8, 972–980. <https://doi.org/10.1038/s41558-018-0299-2>.

Dafka, S., Toreti, A., Zanis, P., Xoplaki, E., Luterbacher, J., 2019. Twenty-first-century changes in the eastern Mediterranean etesians and associated midlatitude atmospheric circulation. *J. Geophys. Res. Atmos.* 124, 12741–12754. <https://doi.org/10.1029/2019JD031203>.

Deryng, D., Conway, D., Ramankutty, N., Price, J., Warren, R., 2014. Global crop yield response to extreme heat stress under multiple climate change futures. *Environ. Res. Lett.* 9, 034011. <https://doi.org/10.1088/1748-9326/9/3/034011>.

Driouech, F., El Rhaz, K., Moufouma-Okia, W., Arjdal, K., Balhane, S., 2020. Assessing future changes of climate extreme events in the CORDEX-MENA region using regional climate model ALADIN-Climate. *Earth Syst. Environ.* 4, 477–492. <https://doi.org/10.1007/s41748-020-00169-3>.

Epstein, Y., Moran, D.S., 2006. Thermal comfort and the heat stress indices. *Ind. Health* 44, 388–398. <https://doi.org/10.2486/indhealth.44.388>.

Faranda, D., Messori, G., Yiou, P., 2017. Dynamical proxies of North Atlantic predictability and extremes. *Sci. Rep.* 7, 41278. <https://doi.org/10.1038/srep41278>.

Giorgi, F., Gutowski, W.J., 2015. Regional dynamical downscaling and the CORDEX initiative. *Annu. Rev. Environ. Resour.* 40, 467–490. <https://doi.org/10.1146/annurev-environ-102014-021217>.

Giorgi, F., Lionello, P., 2008. Climate change projections for the Mediterranean region. *Glob. Planet. Chang.* 63, 90–104. <https://doi.org/10.1016/j.gloplacha.2007.09.005>.

Harpaz, T., Ziv, B., Saaroni, H., Beja, E., 2014. Extreme summer temperatures in the East Mediterranean-dynamical analysis. *Int. J. Climatol.* 34, 849–862. <https://doi.org/10.1002/joc.3727>.

Heaviside, C., Tsangari, H., Paschalidou, A., Vardoulakis, S., Kassomenos, P., Georgiou, K.E., Yamasaki, E.N., 2016. Heat-related mortality in Cyprus for current and future climate scenarios. *Sci. Total Environ.* 569–570, 627–633. <https://doi.org/10.1016/j.scitotenv.2016.06.138>.

Hersbach, H., et al., 2020. The ERA5 global reanalysis. *Q.J.R. Meteorol. Soc.* 146, 1999–2049. <https://doi.org/10.1002/qj.3803>.

Hochman, A., Alpert, P., Harpaz, T., Saaroni, H., Messori, G., 2019. A new dynamical systems perspective on atmospheric predictability: eastern Mediterranean weather regimes as a case study. *Sci. Adv.* 5, eaau0936. <https://doi.org/10.1126/sciadv.aau0936>.

Hochman, A., Mercogliano, P., Alpert, P., Saaroni, H., Bucchignani, E., 2018. High-resolution projection of climate change and extremity over Israel using COSMO-CLM. *Int. J. Climatol.* 38, 5095–5106. <https://doi.org/10.1002/joc.5714>.

Hochman, A., Scher, S., Quinting, J., Pinto, J.G., Messori, G., 2022c. Dynamics and predictability of cold spells over the eastern Mediterranean. *Clim. Dyn.* 58, 2047–2064. <https://doi.org/10.1007/s00382-020-05465-2>.

Hochman, A., Scher, S., Quinting, J., Pinto, J.G., Messori, G., 2021. A new view of heat wave dynamics and predictability over the eastern Mediterranean. *Earth Syst. Dynam.* 12, 133–149. <https://doi.org/10.5194/esd-12-133-2021>.

Kendrovski, V., Baccini, M., Martinez, G.S., Wolf, T., Paunovic, E., Menne, B., 2017. Quantifying projected heat mortality impacts under 21st-century warming conditions for selected European countries. *Int. J. Environ. Res. Public Health* 14, 729. <https://doi.org/10.3390/ijerph14070729>.

Kuglitsch, F.G., Toreti, A., Xoplaki, E., Della-Marta, P.M., Zerefos, C.S., Türkeş, M., Luterbacher, J., 2010. Heat wave changes in the eastern Mediterranean since 1960. *Geophys. Res. Lett.* 37, L04802. <https://doi.org/10.1029/2009GL041841>.

Latt, M.R., Hochman, A., Caldas-Alvarez, A., Helgert, S., Pinto, J.G., Corsmeier, U., 2022. Understanding summer wind systems over the eastern Mediterranean in a high-resolution climate simulation. *Int. J. Climatol.* 42, 8112–8131. <https://doi.org/10.1002/joc.7695>.

Lee, S., Lee, H., Myung, W., Kim, E.J., Kim, H., 2018. Mental disease-related emergency admissions attributable to hot temperatures. *Sci. Total Environ.* 616–617, 688–694. <https://doi.org/10.1016/j.scitotenv.2017.10.260>.

Lielveld, J., Hadjinicolaou, P., Kostopoulou, E., Giannakopoulos, C., Pozzer, A., Tanarhte, M., Tyrllis, E., 2014. Model projected heat extremes and air pollution in the eastern Mediterranean and Middle East in the twenty-first century. *Reg. Environ. Chang.* 14, 1937–1949. <https://doi.org/10.1007/s10113-013-0444-4>.

Lielveld, J., Proestos, Y., Hadjinicolaou, P., Tanarhte, M., Tyrllis, E., Zittis, G., 2016. Strongly increasing heat extremes in the Middle East and North Africa (MENA) in the 21st century. *Clim. Chang.* 137, 245–260. <https://doi.org/10.1007/s10584-016-1665-6>.

Leone, M., et al., 2013. A time series study on the effects of heat on mortality and evaluation of heterogeneity into European and Eastern-Southern Mediterranean cities: results of EU CIRCE project. *Environ. Health* 12, 55. <https://doi.org/10.1186/1476-069X-12-55>.

- Li, D., Bou-Zeid, E., 2013. Synergistic interactions between urban Heat Islands and heat waves: the impact in cities is larger than the sum of its Parts*. *J. Appl. Meteorol. Climatol.* 52, 2051–2064. <https://doi.org/10.1175/JAMC-D-13-02.1>.
- Li, H., Sheffield, J., Wood, E.F., 2010. Bias correction of monthly precipitation and temperature fields from intergovernmental panel on climate change AR4 models using equidistant quantile matching. *J. Geophys. Res.* 115, D10101. <https://doi.org/10.1029/2009JD012882>.
- Lucarini, V., Faranda, D., Moreira Freitas, A.C., 2016. Extremes and Recurrence in Dynamical Systems. John Wiley & Sons, New York, USA <https://doi.org/10.1002/9781118632321>.
- Mora, C., et al., 2017. Global risk of deadly heat. *Nat. Clim. Chang.* 7, 501–506. <https://doi.org/10.1038/nclimate3322>.
- Naim, J.R., Fawcett, R.J.B., 2014. The excess heat factor: a metric for heatwave intensity and its use in classifying heatwave severity. *Int. J. Environ. Res. Public Health* 12, 227–253. <https://doi.org/10.3390/ijerph120100227>.
- Peleg, N., Bartov, M., Morin, E., 2015. CMP5-predicted climate shifts over the East Mediterranean: implications for the transition region between Mediterranean and semi-arid climates. *Int. J. Climatol.* 35, 2144–2153. <https://doi.org/10.1002/joc.4114>.
- Peretz, C., Biggeri, A., Alpert, P., Baccini, M., 2011. The effect of heat stress on daily mortality in Tel Aviv, Israel. *National Security and Human Health Implications of Climate Change.* 241–251. https://doi.org/10.1007/978-94-007-2430-3_20.
- Perkins, S.E., 2015. A review on the scientific understanding of heatwaves—their measurement, driving mechanisms, and changes at the global scale. *Atmos. Res.* 164–165, 242–267. <https://doi.org/10.1016/j.atmosres.2015.05.014>.
- Perkins, S.E., Alexander, L.V., 2013. On the measurement of heat waves. *J. Clim.* 26, 4500–4517. <https://doi.org/10.1175/JCLI-D-12-00383.1>.
- Perkins, S.E., Alexander, L.V., Naim, J.R., 2012. Increasing frequency, intensity and duration of observed global heatwaves and warm spells. *Geophys. Res. Lett.* 39, L20714. <https://doi.org/10.1029/2012GL053361>.
- Pfleiderer, P., Schleussner, C.-F., Kornhuber, K., Coumou, D., 2019. Summer weather becomes more persistent in a 2 °C world. *Nat. Clim. Chang.* 9, 666–671. <https://doi.org/10.1038/s41558-019-0555-0>.
- Robine, J.-M., Cheung, S.L.K., Le Roy, S., van Oyen, H., Griffiths, C., Michel, J.-P., Herrmann, F.R., 2008. Death toll exceeded 70,000 in Europe during the summer of 2003. *Comptes Rendus Biologies* 331, 171–178. <https://doi.org/10.1016/j.crvi.2007.12.001>.
- Russo, S., Sillmann, J., Sterl, A., 2017. Humid heat waves at different warming levels. *Sci. Rep.* 7, 7477. <https://doi.org/10.1038/s41598-017-07536-7>.
- Ruthrof, K.X., et al., 2018. Subcontinental heat wave triggers terrestrial and marine, multi-taxa responses. *Sci. Rep.* 8, 13094. <https://doi.org/10.1038/s41598-018-31236-5>.
- Saaroni, H., Levi, E., Ziv, B., 2018. Particulate matter in the summer season and its relation to synoptic conditions and regional climatic stress – the case of Haifa, Israel. *Water Air Soil Pollut.* 229, 313. <https://doi.org/10.1007/s11270-018-3943-6>.
- Saaroni, H., Savir, A., Ziv, B., 2017. Synoptic classification of the summer season for the Levant using an 'environment to climate' approach. *Int. J. Climatol.* 37, 4684–4699. <https://doi.org/10.1002/joc.5116>.
- Saaroni, H., Ziv, B., Edelson, J., Alpert, P., 2003. Long-term variations in summer temperatures over the eastern Mediterranean. *Geophys. Res. Lett.* 30, 1946. <https://doi.org/10.1029/2003GL017742>.
- Samuelsson, P., Gollvik, S., Jansson, C., Kupiainen, M., Kourzeneva, E., Jan van de Berg, W., 2015. The surface processes of the Rossby Centre regional atmospheric climate model (RCA4). *Meteorology* 157.
- Sohar, E., Birenfeld, C., Shoenfeld, Y., Shapiro, Y., 1978. Description and forecast of summer climate in physiologically significant terms. *Int. J. Biometeorol.* 22, 75–81. <https://doi.org/10.1007/BF01552886>.
- Strandberg, G., et al., 2014. CORDEX scenarios for Europe from the Rossby Centre regional climate model. *RCA4 Report Meteorology and Climatology.* 116.
- Swiss Re Economic Research & Consulting, 2011. *Natural Catastrophes and Man-made Disasters in 2010: A Year of Devastating and Costly Events.* Swiss Reinsurance Company, Zurich, Switzerland.
- Syed, F.S., Latif, M., Al-Maashi, A., Ghulam, A., 2019. Regional climate model RCA4 simulations of temperature and precipitation over the arabian peninsula: sensitivity to CORDEX domain and lateral boundary conditions. *Clim. Dyn.* 53, 7045–7064. <https://doi.org/10.1007/s00382-019-04974-z>.
- Thom, E.C., 1959. The discomfort index. *Weatherwise* 12, 57–61. <https://doi.org/10.1080/00431672.1959.9926960>.
- Trenberth, K., Fasullo, J., Shepherd, T., 2015. Attribution of climate extreme events. *Nat. Clim. Chang.* 5, 725–730. <https://doi.org/10.1038/nclimate2657>.
- van Vuuren, D.P., et al., 2011. The representative concentration pathways: an overview. *Clim. Chang.* 109, 5–31. <https://doi.org/10.1007/s10584-011-0148-z>.
- Wang, L., Chen, W., 2014. Equiratio cumulative distribution function matching as an improvement to the equidistant approach in bias correction of precipitation. *Atmos. Sci. Lett.* 15, 1–6. <https://doi.org/10.1002/asl2.454>.
- Wang, X., Qiu, B., Li, W., Zhang, Q., 2019. Impacts of drought and heatwave on the terrestrial ecosystem in China as revealed by satellite solar-induced chlorophyll fluorescence. *Sci. Total Environ.* 693, 133627. <https://doi.org/10.1016/j.scitotenv.2019.133627>.
- Ward, K., Lauf, S., Kleinschmit, B., Endlicher, W., 2016. Heat waves and urban heat islands in Europe: a review of relevant drivers. *Sci. Total Environ.* 569–570, 527–539. <https://doi.org/10.1016/j.scitotenv.2016.06.119>.
- Zachariadis, T., Hadjinicolaou, P., 2014. The effect of climate change on electricity needs – a case study from Mediterranean Europe. *Energy* 76, 899–910. <https://doi.org/10.1016/j.energy.2014.09.001>.
- Zimmerman, R., Faris, C., 2010. Chapter 4: infrastructure impacts and adaptation challenges. *Ann. N. Y. Acad. Sci.* 1196, 63–86. <https://doi.org/10.1111/j.1749-6632.2009.05318.x>.
- Zittis, G., et al., 2021. Business-as-usual will lead to super and ultra-extreme heatwaves in the Middle East and North Africa. *Npj Clim Atmos Sci* 4, 20. <https://doi.org/10.1038/s41612-021-00178-7>.
- Zittis, G., Hadjinicolaou, P., Fnais, M., Lelieveld, J., 2016. Projected changes in heat wave characteristics in the eastern Mediterranean and the Middle East. *Reg. Environ. Chang.* 16, 1863–1876. <https://doi.org/10.1007/s10113-014-0753-2>.
- Ziv, B., Saaroni, H., 2011. The contribution of moisture to heat stress in a period of global warming: the case of the Mediterranean. *Clim. Chang.* 104, 305–315. <https://doi.org/10.1007/s10584-009-9710-3>.
- Ziv, B., Saaroni, H., Alpert, P., 2004. The factors governing the summer regime of the eastern Mediterranean. *Int. J. Climatol.* 24, 1859–1871. <https://doi.org/10.1002/joc.1113>.